Proceedings of the 3rd IASME/WSEAS Int. Conf. on FLUID DYNAMICS & AERODYNAMICS, Corfu, Greece, August 20-22, 2005 (pp251-256)

Turbulent Flow Simulation over a Wall-mounted Obstacle at Relatively Low Reynolds Numbers

PSYCHOUDAKI S.P., FRAGOS V.P. and LASKOS V.N.
Department of Hydraulics, Soil Science and Agricultural Engineering
Aristotle University of Thessaloniki, 541 24 Thessaloniki, GREECE
papoutsi@agro.auth.gr
http://www.auth.gr/agro.eb/hydraul/intex.htm

Abstract: - In this paper the Navier-Stokes and continuity equations are solved numerically using a DNS turbulent model. The finite element (Galerkin) method is used for a 2D turbulent flow over a wall-mounted obstacle at different Reynolds numbers. The flow characteristics of five different, relatively low Reynolds numbers are studied. The time-mean averaged calculated flow characteristics, such as streamlines, velocity components, wall pressure coefficient, turbulent intensities, Reynolds shear stress and fiction coefficient are presented and discussed. The instantaneous fluctuations of the stream-wise and cross-wise velocities are shown for different Reynolds numbers. The results are discussed with works of other researchers.

Key-Words: Numerical simulation of Navier-Stokes equations, finite element method, two-dimensional turbulent flow, wall-mounted obstacle.

1. Introduction

This paper concerns a numerical simulation of a turbulent, two-dimensional flow over a wall-mounted rectangular obstacle. The fluid is incompressible and Newtonian with constant density. The Navier-Stokes, (N-S), and continuity equations are solved numerically using the Galerkin, finite element method. There are many investigations studying flow over a wall-mounted obstacle or a backward-facing step numerically [1, 2, 3, 4, 6, 7, 8, 10, 11, 12 and others] and experimentally [1, 2, 12, and others]. Many simulation models have been applied to N-S equations, such as finite volume [3, 7], model of vorticity [6], k-ε model [1], direct numerical simulation (DNS) [4, 5, 8, 9, 10, 11], and others. There are also many numerical methods used to solve N-S equations, as, altering-direction-implicit (ADI) method [6], second order central differencing method [7], second order of QUICK and SIMPLEC method [3], finite difference method [1, 2, 8] and finite element method [4, 9, 10, 11].

The present work studies a 2D incompressible flow of relatively low Reynolds numbers, from 1304 up, to 2200. The Reynolds numbers, $(Re)_h$, are calculated with respect to the obstacle's height and the inlet free stream velocity. Five different Reynolds numbers are used. The idea of this work was to study the flow characteristics according to Reynolds number. The model of Direct Numerical Simulation, (DNS), is chosen because it can calculate small and large vortices due to the small size of time step, Δt, and grid spacing Δx and Δy. As it has been said, the Galerkin .numerical method is used.

2. Governing Equations

The flow has been simulated in a wind tunnel and is nominated to be 2D and turbulent over a rectangular mounted-obstacle. There is also no gravity or other external power influences upon the flow. The flow domain is shown in Fig. 1.

The Navier-Stokes and continuity equations, for the described flow, in non-dimensional form are,

$$\frac{\partial \vec{V}}{\partial t} + (\vec{V}\vec{\nabla})\vec{V} = -\vec{\nabla}p + \frac{1}{\mathrm{Re}}\nu\vec{\nabla}^2\vec{V} \qquad (1)$$

$$\vec{\nabla}\vec{V} = 0 \qquad (2)$$

The boundary conditions upstream of the entrance of the computational domain are a uniform free stream. The no-slip boundary conditions are imposed along the walls of the wind tunnel and the obstacle. The outlet boundary condition is a free boundary condition which lets the fluid leave the

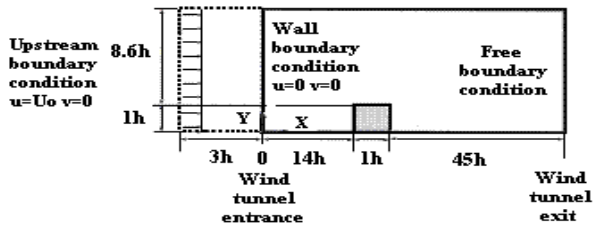

Figure 1. Computational domain of nominally two dimensional flow over a mounted obstacle.

computational domain freely without any distortions, [4, 9]. The initial condition is given by solving the 2D N-S equations at t=0 and $(Re)_h$=1, for $(Re)_h$=1304. For the next flow of $(Re)_h$=1500 the time mean-averaged solution of $(Re)_h$=1304 is used. The same way is used to calculate the initial condition of the other flows. That is, the flows of $(Re)_h$=1800, 2000 and 2200 have as initial conditions the time mean-averaged solutions of $(Re)_h$=1500, 1800 and 2000, respectively.

2.1 Finite Element Formulation - Spatial and Time Advancements

To solve the governing equations (1) and (2), the finite element method has been used. The pressure is formulated by a linear basic function, while the velocity by a quadric. The unknown velocities and pressure are expanded in Galerkin basic functions. Equations (1) and (2) are weighted integrally with the basic functions. Finally, applying the divergence theory, the following weight residuals are received,

$$R_c^i = \int_{\forall} \vec{\nabla}\vec{V}\psi^i d\forall \qquad (3)$$

$$R_M^i = \int_{\forall} [\frac{\partial \vec{V}}{\partial t} + \vec{V}\vec{\nabla}\vec{V} - \vec{\nabla}(-pI + \frac{1}{\mathrm{Re}}T)]\Phi^i d\forall \qquad (4)$$

Where $\vec{V}$ is the vector of velocity, I is the identity matrix, $T = \nabla\vec{V} + (\nabla\vec{V})^T$ is the stress tensor of the Newtonian fluid with $\nabla^2\vec{V} = \nabla T$, $d\forall$ is the infinitely small volume of calculating domain and Ψ^i, Φ^i are the linear and quadratic basic functions in equations (3) and (4) respectively.

The non linear system of equations (3) and (4) is solved numerically with the Newton-Raphson method. The flow domain is tessellated in 14645 finite elements with 59299 nodes and 133603 unknowns. The time-step is fixed at Δt=0.01 h/U_o. At each space-point 15.000 instant samples are computed at a total time T=150. Each time- step needs three runs to converge. The biggest error of Newton-Raphson method is 10^{-6} for velocities and $5x10^{-4}$ for pressure calculations. Each run uses 2 CPU, minutes.

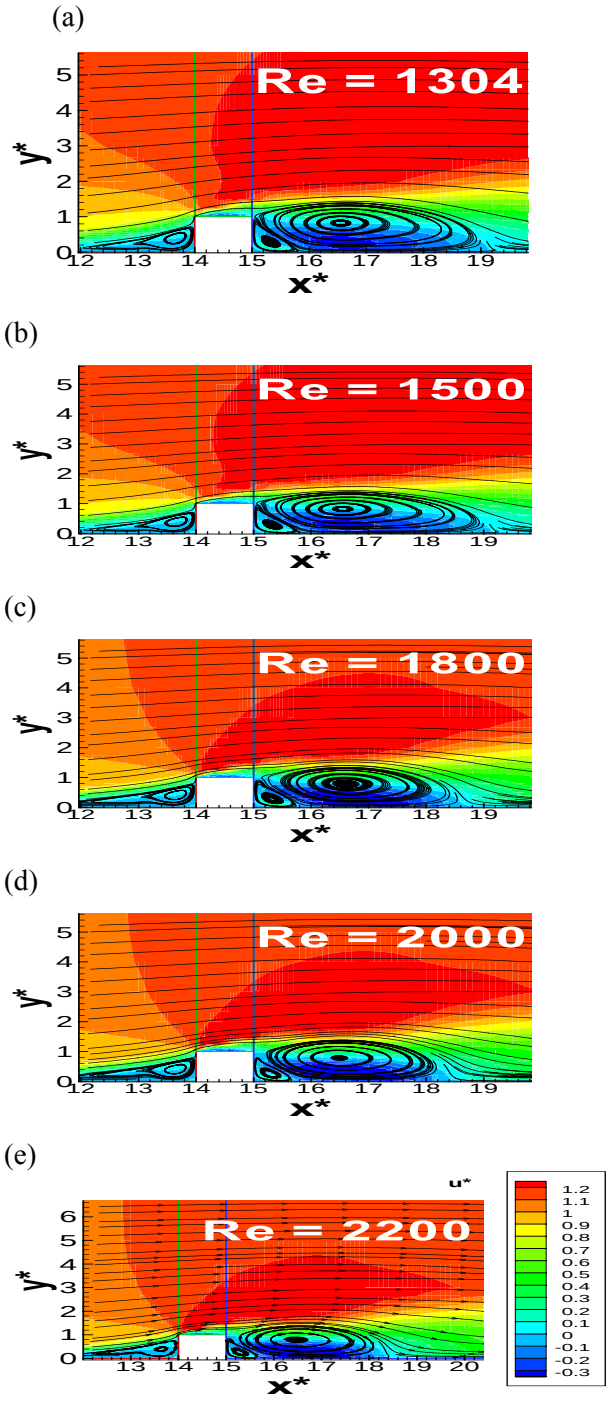

Figures 2 a,b,c,d,e. Computed time-mean averaged streamlines at different Reynolds numbers.

3. Results and Discussion

The calculated time-mean averaged streamlines for five different Reynolds numbers ($(Re)_h$ = 1304, 1500, 1800, 2000 and 2200) are shown in Fig. 2. It can be observed that the shape of the re-circulated

flow upstream of the obstacle increases as the Reynolds number increases but the shape of the recirculation zone is decreasing. That means that the separation distance is increasing while the reattaching distance is decreasing as the Reynolds number is increasing. Armaly et al. [2] in their experimental results and numerical predictions show that the reattachment distance downstream of a backward-facing step is decreasing for 1200<Re<6600. The present work is in the range of these Reynolds numbers. The colour indication refers to the value of the time-mean averaged stream-wise velocity in the computational domain. It can be seen that increase of the Reynolds number, the region, where the maximum velocity occurs over the obstacle, is increasing.

Figures 3a,b and 4a,b show time-mean averaged stream-wise and cross-wise velocity profiles for different Reynolds numbers respectively. The stream-wise velocity profiles are identical upstream, (not shown), and on the top of the obstacle, (Fig. 3a), but there are differences downstream of it in the recirculation region and further on, which are visible when Fig. 3b is enlarged. The cross-wise velocity distributions upstream of the obstacle for $(Re)_h$=1304 does not follow the same pattern as the other four $(Re)_h$. On the top and downstream of the obstacle, Figs 4a,b, the velocity distributions are similar as far as the Reynolds numbers are concerned, except of the value of the maximum (or the minimum) close to the wall.

Figures 5 show the instantaneous stream-wise, Figs 5a,b,c, and cross-wise, Figs 5d,e,f, velocity fluctuations. These velocity fluctuations concern three positions along x^* axis, one upstream of the obstacle and close to separation at a height twice as high as the height of the obstacle, (x^*=12 and y^*=2), and two downstream of reattachment, (x^*=30 and 40 (or x=15h and 25h)) and as high as the center of the tunnel, (y^*=5). The flow is turbulent far downstream of the obstacle and up to the middle of the tunnel height, as it is shown in Figs 5b,c,e,f. It should be noticed, that there are strong inlet effects in the stream-wise velocity fluctuations in all three positions for the Reynolds number equal to 1304, while these effects are not strong in the other four Reynolds numbers. In the cross-wise velocity fluctuations the strong inlet effects are shown only at the position x^*=12. This effect is caused by the initial condition. Another inlet effect which needs a dimensionless, computational time equal to about, t^*=60, for $(Re)_h$ =1304 is also shown, while for the other four flows the time is equal to about

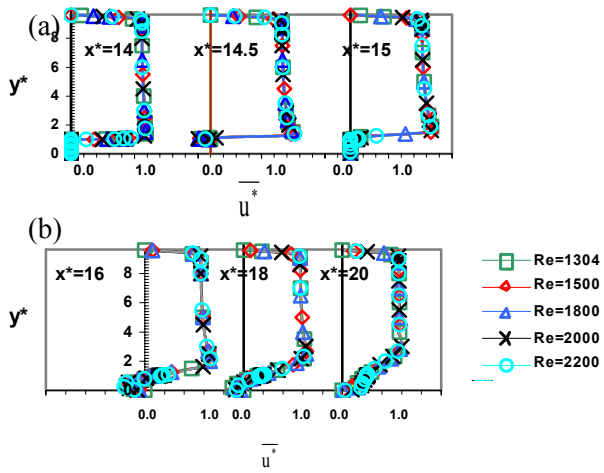

Figures 3 a,b. Time-mean averaged stream-wise velocity profiles for different Reynolds numbers, (a) on the top, (b) downstream of the obstacle.

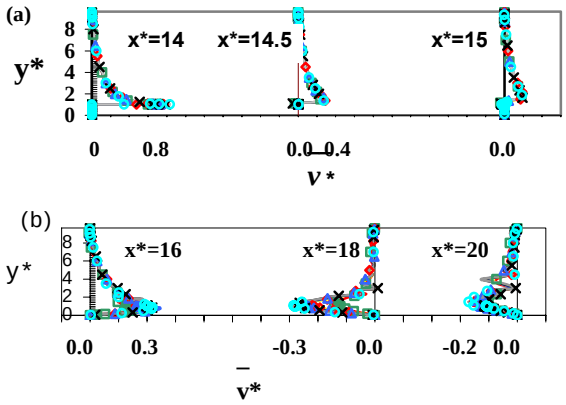

Figures 4 a,b. Time-mean averaged cross-wise velocity profiles for different Reynolds numbers, (a) on the top, (b) downstream of the obstacle.

t^*=40, to get a turbulent signal. This inlet effect is due to inlet boundary condition. This time is smaller than the time discussed by Le et al. [8].

Figures 6a,b and 7a,b respectively, show respectively, predicted stream-wise and cross-wise, turbulent intensities for different Reynolds numbers and positions. The stream-wise turbulent intensities of $(Re)_h$=1304 at the positions upstream of the obstacle have shown differences to all the other Reynolds numbers, (not shown). These differences are small in the cross-wise turbulent intensities. The differences shown in the stream-wise velocity fluctuations and the turbulent intensities are due to the initial condition of the flow of $(Re)_h$= 1304. This initial condition is based on a flow with a much smaller Reynolds number than the others, as it is referred in section 2. The influence of the initial condition to the flow and the difference between the Reynolds numbers is a subject that should be investigated. The same comments as

before are applied to the distributions of the Reynolds stresses at different positions and Reynolds numbers, Figs 8a,b.

There are also differences of the maximum intensity values close to the wall, on the top and downstream of the obstacle in the recirculation region, for both intensities.

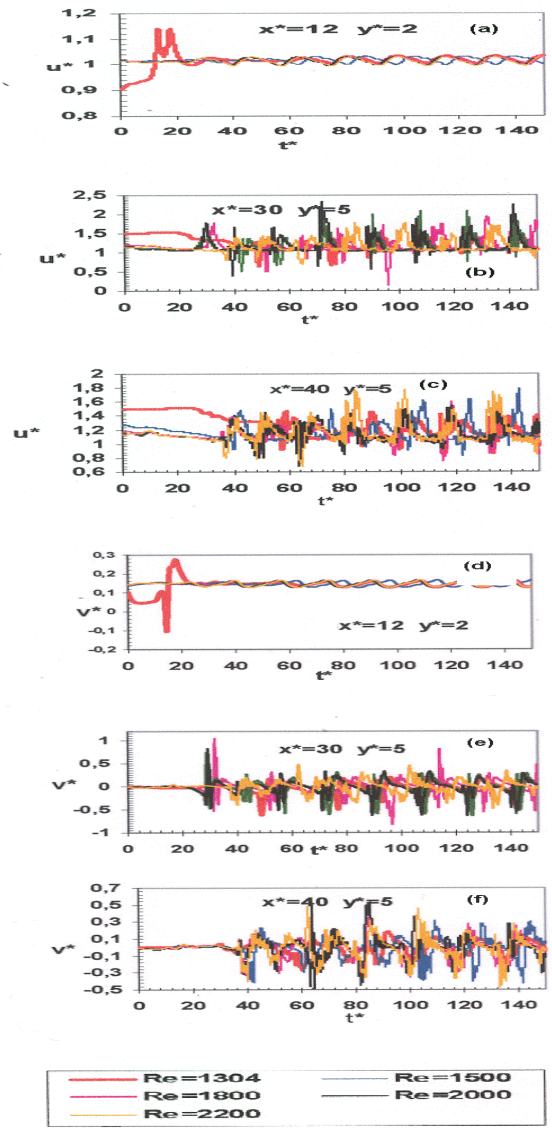

Figures 5 a,b,c,d,e,f. Instantaneous stream-wise and cross-wise velocity fluctuations for different Reynolds numbers.

Figures 9a,b,c show predicted distribution of the pressure coefficient, (a) on the top and (b) downstream of the obstacle, for different Reynolds numbers. Figures 9a,b show that the pressure coefficient is increasing with the increase of the Reynolds number. Figure 9c shows the distribution of calculated pressure distribution by Le et al. [8]

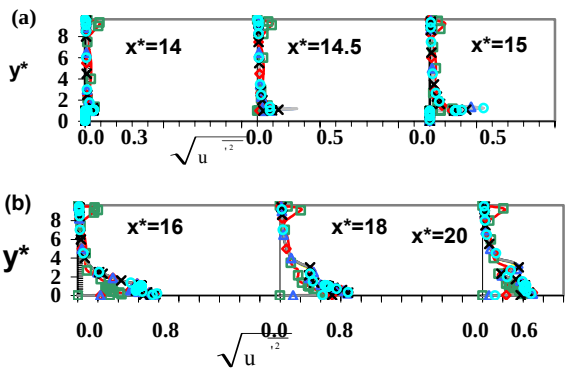

Figures 6 a,b. Predicted stream-wise turbulent intensities for different Reynolds numbers. Legend as Figs 3a,b.

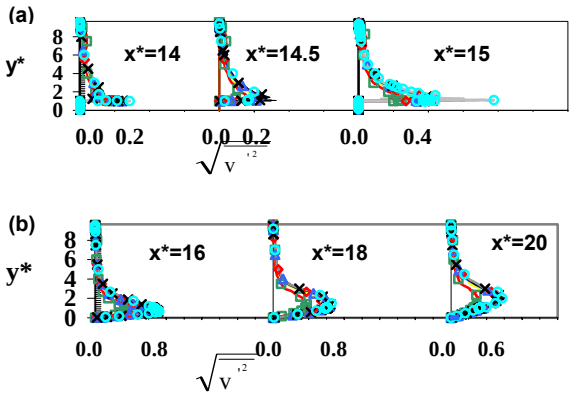

Figures 7 a,b. Predicted cross-wise turbulent intensities for different Reynolds numbers. Legend as Figs 3a,b.

with the experimental results by Jovic and Driver [8, (1994)] downstream of a step-wall, $(Re)_h$=5100. Qualitative comparison between Figs 9b and 9c shows many similarities.

The skin–friction coefficient is given by $C_f = \frac{2\tau_w}{\rho U_o^2} = 2\bar{\tau}_w^*$, while the non-dimensional wall shear-stress by $\bar{\tau}_w^* = \frac{1}{(Re)_h}(\frac{\partial \bar{u}^*}{\partial y^*} + \frac{\partial \bar{v}^*}{\partial x^*})$. Figures 10 a,b show the computed skin-friction coefficient on the top and downstream of the obstacle. It is shown that the skin-friction coefficient has a minimum value at the upper edge of the obstacle, (Fig. 10a). Figure 10b shows a similar, as Fig 10a, distribution of skin-friction coefficient for different $(Re)_h$, downstream of the obstacle. Qualitative comparison of skin-friction coefficient computed by Le et al [8] and measured by Jovic and Driver [8, (1994)] (downstream of a step) with the present work (downstream of an obstacle) are shown between Figs 10b and 10c. The similarities are obvious though there are differences in the values of the distribution. It is supposed, that the

difference of the values is owed to the way of calculation of the wall shear-stress.

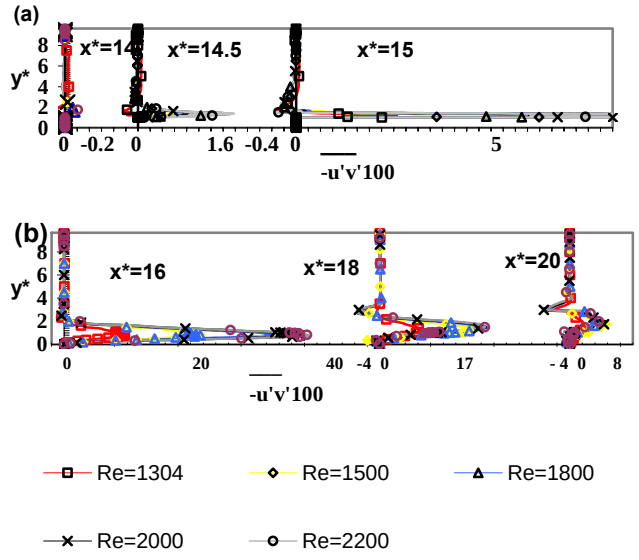

Figures 8 a,b,c. Predicted Reynolds stresses at different positions and Reynolds numbers.

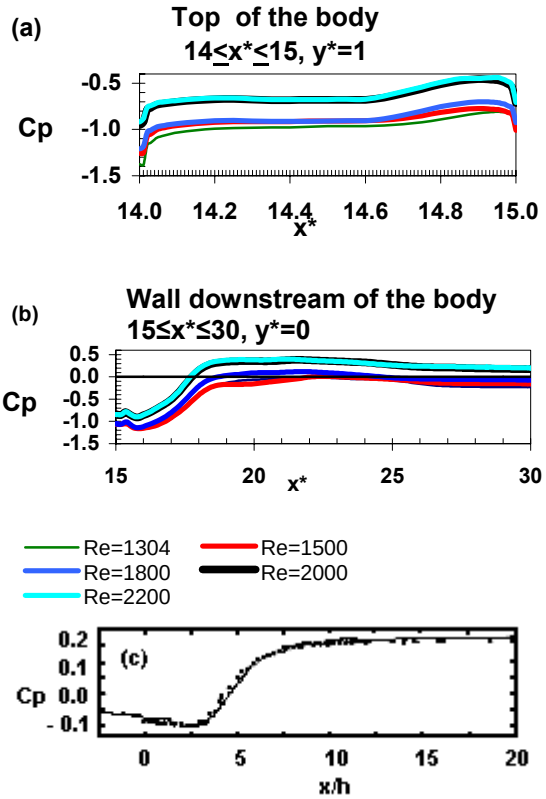

Figures 9 a,b,c. Wall pressure coefficient. (a),(b) Present work, (c) Le et al [8] and Jovic and Driver [8 (1994)], downstream of the step. Fig.9c, to be compared to the present work, Fig. 9b.

4. Conclusion

The paper studies a nominated 2D, turbulent flow over a wall-mounted rectangular obstacle. The fluid is incompressible and Newtonian with constant density. No gravity or other external power influences the flow. The Direct Numerical Simulation Model is used to solve the Navier-Stokes equations with the Galerkin method. Five different Reynolds numbers are used from $1304<(Re)_h<2200$. A uniform free stream flow is imposed upon the entrance of the tunnel, the no-slip boundary conditions are applied along the walls of the tunnel and the obstacle and the free boundary condition is applied at the exit of the tunnel. As initial condition, a laminar flow solution at $t = 0$

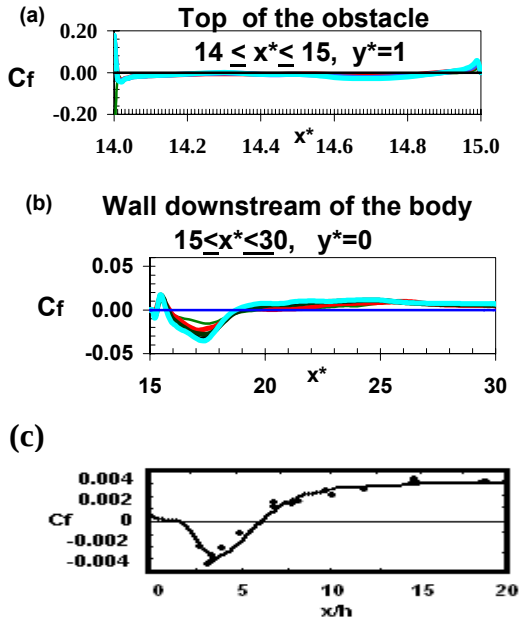

Figures 10 a,b,c. Computational distribution of skin-friction coefficient. Present work (obstacle), (a),(b). Legend as Figs 9a,b. Qualitative comparison of (b) with Le et al [8] and Jovic and Driver [8 (1994)] (step), (c).

and $(Re)_h=1$ is used for the flow of $(Re)_h=1304$. In the next flow of $(Re)_h=1500$, the time mean-averaged solution of $(Re)_h=1304$ is used as initial condition. The initial conditions of the other flows of $(Re)_h=1800$, 2000 and 2200 have also as initial conditions the time mean-averaged solutions of $(Re)_h=1500$, 1800 and 2000 respectively.

The calculated time-mean averaged streamlines show that the length of the recirculated flow upstream and downstream of the obstacle changes with the Reynolds number. The length of separation increases with the increase of $(Re)_h$, while the length of reattachment decreases. The above mentioned statement about the reattachment length is verified by Armaly et al. [2] in their experimental and computational work. The time-mean averaged stream-wise velocity profiles are identical upstream and on the top of the obstacle

but the profiles downstream of it show differences. The cross-wise velocity profiles are similar for all flows except of the flow of $(Re)_h$=1304. Differences are also shown in the maximum (or minimum) values of the velocity close to the wall.

The instantaneous stream-wise and cross-wise velocity fluctuations show that the flow is turbulent far downstream of the obstacle and up to the middle of the tunnel height. Two strong inlet effects, in the stream-wise velocity fluctuations are present. The first is shown in the flow of $(Re)_h$=1304 and has to do with the initial condition. The other inlet effect is shown to all other flows and has to do with the inlet boundary condition. It seems that a computational time of about t*=40 or 60 is needed to get a turbulent signal.

The predicted stream-wise and crosswise turbulent intensities show differences between $(Re)_h$=1304 and all the other Reynolds numbers upstream of the obstacle. It is supposed that this is due to the initial condition of the flow $(Re)_h$=1304. This "initial condition" effect is not seen in the stream-wise velocity profiles, it is slightly visible in the crosswise velocity profiles upstream of the obstacle but it is clearly seen in the velocity fluctuations. Differences, between the $(Re)_h$=1304 and all the other Reynolds numbers show the predicted Reynolds stresses, too. It is believed that they are also due to the "initial condition" effect mentioned above. The pressure coefficient on the top and downstream of the obstacle is increasing with the increase of Reynolds number. Predicted distributions of the pressure coefficient downstream of the obstacle compared qualitatively to the predicted pressure coefficient by Le et al. [8] and the measured one by Jovic and Driver [8, (1994)] downstream of a step-wall, show many similarities.

The distribution of skin-friction coefficient for different $(Re)_h$, on the top and downstream of the obstacle are similar. The values, of the computed skin-friction coefficient on the above mentioned positions, seem to be affected by the way of calculation of the wall shear-stress. Qualitative comparison of the calculated skin-friction coefficient, by Le et al. [8], as well as the measured one, by Jovic and Driver [8, (1994)] downstream of a step to the flow of the present work, shows similarities.

References

[1] Acharya S., Dutta S., Myrum T.A. and Baker R.S., Turbulent Flow past a Surface-Mounted Two-Dimensional Rib, *ASME J. Fluids Eng.*, Vol. 116, 1994, pp. 238-246.

[2] Armaly B. F., Durst F., Pereira J. C. F. and Scoenung B., Experimental and Theoretical Investigation of Backward-facing Step Flow, *J. Fluid Mech.*, Vol. 127, 1983, pp. 473-496.

[3] Boum Ngo G.B., Martemianov S., Alemany A., Computational Study of Laminar Flow and Mass Transfer around a Surface-mounted Obstacle, *Int. J. Heat and Mass Transfer,* Vol. 42, 1999, pp. 2849-2861.

[4] Fragos V.P., Psichoudaki S.P. and Malamataris N.A., Direct Computation of Turbulent Flow over a Surface Mounted Obstacle, *1st Int. Conf. "From Scientific Computing to Computational Engineering", Athens, Greece, 8-10 Sept,. 2004*.

[5] Friedrich R., Huttl T.J., Manhart M. and Wagner C., Direct Numerical Simulation of Incompressible Flows, *Computers and Fluids*, Vol. 30, 2001, pp.555-579.

[6] Hong Ying-Jong, Hsieh Shou-Shing and Shih Hnei-Jan, Numerical Computation of Laminar Separation and Reattachment of Flow over Surface mounted Ribs, *Transactions of the ASME, J. Fluids Eng.,* Vol. 113, 1991, pp. 190-198.

[7] Hwang J.Y., Yang K.S., Numerical Study of Vortical structures around a wall – mounted cubic obstacle in channel Flow, *Physics of Fluids*, Vol. 6, N7, 2004, pp. 2382-2394.

[8] Le H., Moin P. and Kim J., Direct Numerical Simulation of Turbulent Flow over a Backward-facing Step, *J. Fluid Mech.*, Vol. 330, 1997, pp. 349-794.

[9] Malamataris N.A., *Computed-aided Analysis of Flows on Moving and Unbounded domains: Phase-change Fronts and Liquid Leveling*, Ph. D. Thesis, Univ. of Mich. Ann Arbor, 1991.

[10] Psychoudaki S.P., Fragos V.P. and Malamataris N., Numerical Study of separating and Reattaching Flow over a Rectangular Wall-mounted Obstacle, *3rd IASME/WSEAS Int. Conf. on Fluid Mechanics and Aerodynamics*, Corfu Island, Greece, August 20-22, 2005.

[11] Psychoudaki S.P., Laskos V.N. and Fragos V.P., A Two-dimension Computational Investigation of the Flow over a Wall-mounted Parabolic Body, *3rd IASME/WSEAS Int. Conf. on Fluid Mechanics and Aerodynamics*, Corfu Island, Greece, August 20-22, 2005.

[12] Yaghoubi M. and Mahmoodi S., Experimental Study of Turbulent Separated and Reattached Flow, over a Finite Blunt Plate, *Experimental Thermal and Fluid Science*, Vol. 29. 2004, pp. 105-112.